Polarization dependence of the propagation constant of leaky guided modes

Adi Pick[1,2,*] and Nimrod Moiseyev[1,3]
[1]*Faculty of Chemistry, Technion-Israel Institute of Technology, Haifa 32000, Israel*
[2]*Faculty of Electrical Engineering, Technion-Israel Institute of Technology, Haifa 32000, Israel*
[3]*Faculty of Physics, Technion-Israel Institute of Technology, Haifa 32000, Israel*

(Received 31 January 2018; published 24 April 2018)

We show that transverse-magnetic (TM) leaky modes can propagate further than transverse electric (TE) modes in real-index dielectric waveguides. We compute the density of states and find that while the TE spectrum contains only overlapping resonances, the TM spectrum typically contains several isolated peaks. By transforming the TM equation into a Schrödinger-type equation, we show that these isolated peaks arise due to δ-function barriers at the core-cladding interface. Our theory is useful for a range of applications, including filtering TM modes from initially unpolarized light and transferring information between distant waveguides.

DOI: 10.1103/PhysRevA.97.043854

I. INTRODUCTION

The analogy between Maxwell's equations for light propagation in lossy waveguides and non-Hermitian quantum mechanics [1–4] has lead to the discovery of many intriguing phenomena, such as loss-induced transparency [5], gain-induced suppression of lasing [6], unidirectional invisibility [7], adiabatic optical switches [8,9], and sensors with sublinear sensitivity [10]. In this work, we report yet another intriguing property of non-Hermitian waveguides, which stems from the analogy to quantum mechanics: transverse-magnetic (TM) leaky modes can propagate further than transverse-electric (TE) modes along real-index thin waveguides, and are more suitable for applications which require isolated resonances.

In the most simple picture, an optical fiber consists of a high-index material (core) coated by a lower-index material (cladding) [11]. In the absence of loss or gain, light at certain frequencies and wavelengths is confined to propagate inside the core due to total internal reflection at the core-cladding interface [12]. These are the so-called *confined guided modes*, which propagate along the fiber while accumulating an overall phase of $e^{i\beta_n z}$ with a real propagation constant β_n. However, in the presence of material absorption, radiation loss, or gain, light can be attenuated or amplified upon propagation. In such cases, the propagation constant β_n is complex [13], and the modes are called *leaky guided modes* [14]. When the light intensity is attenuated along the propagation direction, it grows unboundedly in the transverse direction [as follows from the dispersion relation, Eq. (10)]. This divergence poses many theoretical challenges, such as finding a proper way to normalize the modes [15–17] and revisiting various expressions from "Hermitian optics" [18,19]. While most previous work on complex-propagation constants typically involves gain or loss in the waveguide [20–23], we explore in this work the less familiar case, where β_n is complex solely due to radiation losses in the transverse direction [24]. In the latter type of modes, β_n strongly depends on the polarization and, consequently, the polarization can be used as a knob to control the propagation.

Despite the long-standing debate on the interpretation, completeness, and normalization of leaky modes [15,16], there is no question about their usefulness when it comes to describing light at nearly resonant wave vectors and in close proximity to the waveguides. Most importantly, the complex propagation constants β_n determine the location of peaks in the density states. This is similar to non-Hermitian quantum mechanics, where resonant complex eigenenergies, $E_n = \varepsilon_n - i\Gamma_n$, represent peaks in the density of continuum states, centered around real energies ε_n with width Γ_n [25]. In this work, we use the term *isolated resonances* when the peaks do not overlap (or, more formally, when $|\varepsilon_{n+1} - \varepsilon_n| > \Gamma_n, \Gamma_{n+1}$).

Figure 1 summarizes the main result of this paper: the existence of narrow TM resonances in real-index dielectric waveguides. We analyze the rectangular waveguide shown in Fig. 1(a). Since the system has mirror-plane symmetry around $z = 0$, the waveguide can support either TE or TM modes, in which the electric or magnetic fields are transverse to the direction of propagation. In Sec. II, we review the scalar Maxwell equations for TE and TM polarizations [Eq. (4) and Eq. (8), respectively] and in Sec. III, we present their solution, which demonstrates the polarization dependence of the propagation constants. Figure 1(b) shows contour plots of the solutions of the transcendental equations from Sec. III [Eqs. (12)–(15)], whose zeros are the TE and TM resonant propagation constants (also known as the poles of the scattering matrix [26]). Clearly, the TM resonances are situated closer to the real axis and are, therefore, more strongly confined to the waveguide. We explain this result in Sec. IV, by using the analogy between Maxwell's equations and the Schrödinger equation. In Sec. V, we explore an important consequence of narrow TM resonances: appearance of isolated peaks in the TM density of states [as shown in Fig. 1(c)]. In Sec. VI, we describe two possible applications of our theory for filtering

*adipick@technion.ac.il

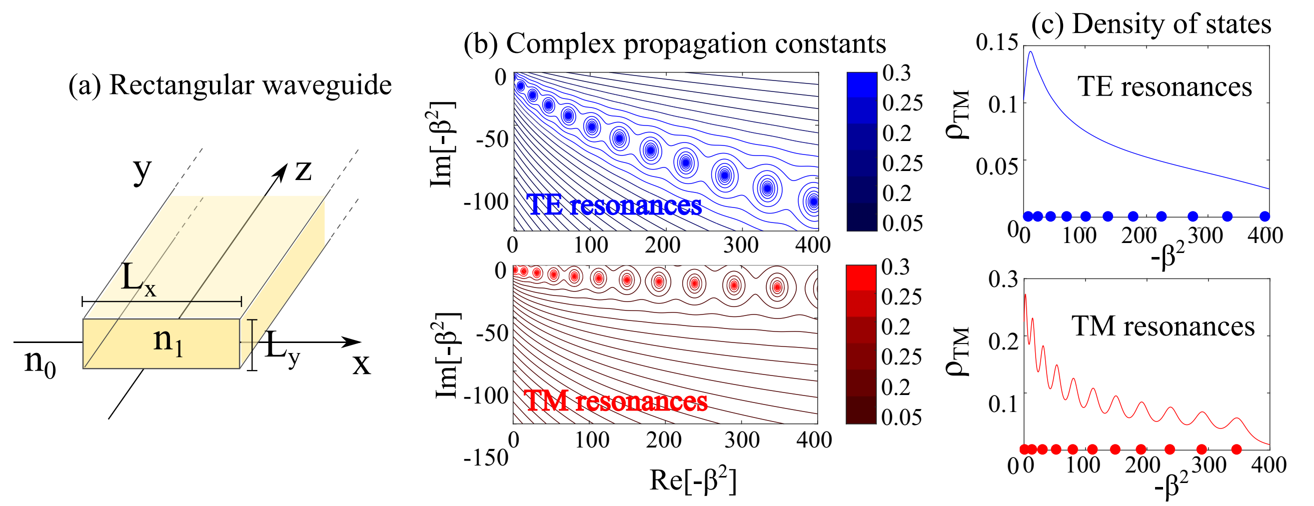

FIG. 1. (a) Dielectric waveguide with a thin rectangular cross section ($L_x \gg L_y$ and $L_x = 1\ \mu$m) and index $n_1 = \sqrt{2}$ surrounded by air with index $n_0 = 1$. The wavelength of light is $\lambda = \frac{2\pi c}{\omega} = 3\ \mu$m. (b) TE and TM complex propagation constants for the structure from (a). The plots depict contours of the functions $\Delta_{\rm TE}(\beta^2)$ (top) and $\Delta_{\rm TM}(\beta^2)$ (bottom) (defined in text), whose poles are the resonant wave vectors (also known as the poles of the scattering matrix [26]). (c) Density of states, evaluated using Eq. (20), for TE (top) and TM (bottom) polarizations. The dots mark the real parts of propagation constants from (b).

TM modes from initially unpolarized light and for transferring information between distant waveguides.

II. SCALAR MAXWELL EQUATIONS

Our starting point is the frequency-domain Maxwell equations for nonmagnetic media [12]: $\nabla \times \mathbf{E} = i\omega\mu_0\mathbf{H}$ and $\nabla \times \mathbf{H} = -i\omega\varepsilon_0\varepsilon\mathbf{E}$. Here, $\mathbf{E}$ and $\mathbf{H}$ are the electric and magnetic vector fields, ε_0 and μ_0 are the vacuum permittivity and permeability, and ε is the relative permittivity of the medium (the relative permeability in non-magnetic media is 1). From Maxwell's equations, one can obtain two decoupled wave equations for the electric and magnetic fields [12]:

$$\nabla \times \nabla \times \mathbf{E} = \left(\frac{\omega}{c}\right)^2 \varepsilon\,\mathbf{E}, \tag{1}$$

$$\nabla \times \frac{1}{\varepsilon}\nabla \times \mathbf{H} = \left(\frac{\omega}{c}\right)^2 \mathbf{H}, \tag{2}$$

where $c = 1\sqrt{\varepsilon_0\mu_0}$ is the speed of light. Due to the symmetry of the geometry under study [Fig. 1(a)], the polarization of the modes is either TE (with nonzero field components E_y, H_x, and H_z) or TM (with nonzero H_y, E_x, and E_z). This property allows one to reduce Maxwell's vectorial equations [Eq. (1) and Eq. (2)] to scalar equations for the electric and magnetic fields.

In order to study polarization dependence of the propagation constant, we focus on ultra-thin rectangular waveguides, which are known to have record-low losses [27,28]. In this limit [i.e., when $L_x \gg L_y$ using the definitions of Fig. 1(a)] the y dependence of the field can be neglected. The electric and magnetic modes have the form

$$\psi(x,z) = e^{i\beta z}\psi(x), \tag{3}$$

and the propagation constant β is generally complex. Focusing first on TE polarization, we substitute $E_y = e^{i\beta z}e_y(x)\hat{y}$ into Eq. (1), introduce the index of refraction $n^2 = \varepsilon$, and obtain

$$\left[\frac{d^2}{dx^2} + \left(\frac{\omega}{c}\right)^2 n^2(x)\right] e_y(x) = \beta^2 e_y(x). \tag{4}$$

This equation is formally equivalent to the time-independent Schrödinger equation of a one-dimensional particle:

$$\left[-\frac{\hbar^2}{2m}\frac{d^2}{dx^2} + V(x)\right]\psi(x) = E\psi(x), \tag{5}$$

with $m = 0.5$, $\hbar = 1$, $E = -\beta^2$, and potential field

$$V_{\rm TE}(x) = -\left(\frac{\omega}{c}\right)^2 n^2(x). \tag{6}$$

The situation is quite different for TM polarization. Substituting $H_y = e^{i\beta z}h_y(x)\hat{y}$ into Eq. (2), one finds that the magnetic field satisfies the scalar equation

$$-\frac{d}{dx}\frac{1}{\varepsilon}\frac{d}{dx}h_y + \beta^2\frac{1}{\varepsilon}h_y = \left(\frac{\omega}{c}\right)^2 h_y, \tag{7}$$

or alternatively [11]

$$\left[\frac{d^2}{dx^2} + \left(\frac{\omega}{c}\right)^2 n^2(x) - \frac{d\,\ln n^2(x)}{dx}\frac{d}{dx}\right] h_y(x) = \beta^2 h_y(x). \tag{8}$$

(For details on how to obtain this result, see [29].) The last term in square brackets contains a spatial derivative and, therefore, cannot be interpreted as the potential of a conservative force. In Sec. IV, we transform Eq. (8) into an equivalent

Schrödinger-type equation with an effective conservative potential and show that this term is responsible for the narrow TM resonances.

III. CONFINED AND LEAKY MODES

Our example system from Fig. 1(a) can be solved semianalytically using standard techniques from quantum mechanics [30]. The eigenmodes of a piecewise homogeneous potential are outgoing plane-wave solutions, whose coefficients are determined by matching the field and its derivatives at the boundaries. Since our example problem is symmetric under reflection around $x = 0$, it is convenient to use the ansatz

$$\psi(x) = \begin{cases} e^{-iqx}, & \text{for } x < -\frac{L}{2}, \\ A\cos(k_x x) + B\sin(k_x x), & \text{for } |x| < \frac{L}{2}, \\ e^{iqx}, & \text{for } x > \frac{L}{2}, \end{cases} \tag{9}$$

where even and odd solutions have $B = 0$ and $A = 0$, respectively. Here, ψ is either E_y (for TE modes) or H_y (for TM modes) and the x components of the wave vectors in the core and cladding, k_x and q, are related to the propagation constant, β, via the dispersion relations

$$k_x^2 + \beta^2 = \left(\frac{\omega}{c}\right)^2 \varepsilon_1, \tag{10}$$

$$q^2 + \beta^2 = \left(\frac{\omega}{c}\right)^2 \varepsilon_0. \tag{11}$$

Since the TE equation [Eq. (4)] is equivalent to a one-dimensional particle in a box, the boundary conditions are continuity of the field (ψ) and its derivative ($d\psi/dx$) at the core-cladding interface ($x = \pm L/2$). By demanding continuity of ψ and $d\psi/dx$ for the ansatz solution [Eq. (9)] and using the dispersion relations [Eq. (10) and Eq. (11)] to express q in terms of k_x, one obtains the well-known transcendental equations [11]:

$$\text{Even TE modes}: \tan\left(\frac{k_x L}{2}\right) = -i\sqrt{1 - \frac{\omega^2(\varepsilon_1 - \varepsilon_0)}{(ck_x)^2}}, \tag{12}$$

$$\text{Odd TE modes}: -\cot\left(\frac{k_x L}{2}\right) = -i\sqrt{1 - \frac{\omega^2(\varepsilon_1 - \varepsilon_0)}{(ck_x)^2}}. \tag{13}$$

In contrast, the TM equation [Eq. (8)] contains an additional derivative term which changes the boundary conditions. In order to derive the correct boundary conditions, one can integrate Eq. (7) over an infinitesimal region around the boundary (at $x = \frac{L}{2}$). The first term on the left-hand side gives

$$\lim_{\delta \to 0} \int_{\frac{L}{2}-\delta}^{\frac{L}{2}+\delta} dx \frac{d}{dx}\frac{1}{\varepsilon}\frac{dh_y}{dx} = \frac{h'_y(L/2)_{\text{out}}}{\varepsilon(L/2)_{\text{out}}} - \frac{h'_y(L/2)_{\text{in}}}{\varepsilon(L/2)_{\text{in}}}$$

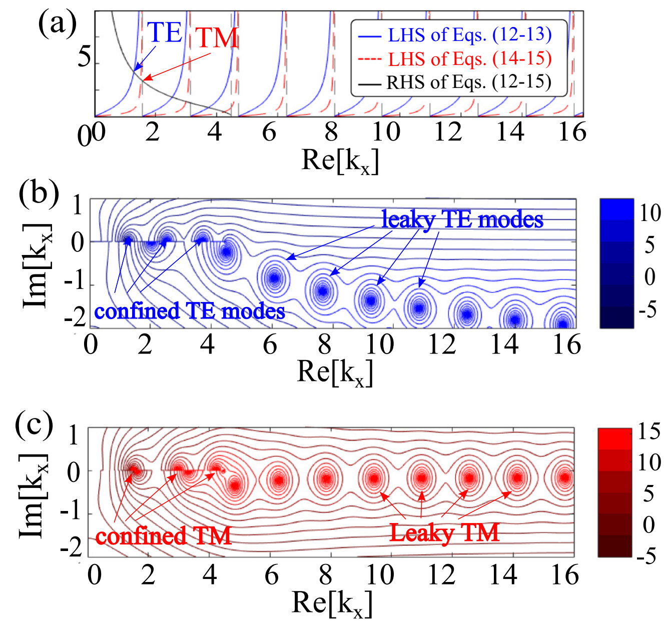

FIG. 2. (a) Right- and left-hand sides of the transcendental Eqs. (12)–(15) for the structure from Fig. 1(a) (with $n_0 = 1, n_1 = \sqrt{2}$, and $\frac{\omega L}{2\pi c}$). The intersections of the blue-solid (red-dashed) curves with the black curve define the transverse wave vectors $[k_x^{\text{con}}]_n$ of TE (TM) confined guided modes. Panels (b) and (c) show contours of the functions $\Delta_{\text{TE}}(k_x)$ and $\Delta_{\text{TM}}(k_x)$, respectively (defined in the text), whose complex poles are the transverse wave vectors of confined and leaky TE or TM modes.

and the remaining terms vanish. Therefore, the TM transcendental equations are [11]

$$\text{Even TM modes}: \frac{\varepsilon_0}{\varepsilon_1}\tan\left(\frac{k_x L}{2}\right) = -i\sqrt{1 - \frac{\omega^2(\varepsilon_1 - \varepsilon_0)}{(ck_x)^2}}, \tag{14}$$

$$\text{Odd TM modes}: \frac{\varepsilon_0}{\varepsilon_1} - \cot\left(\frac{k_x L}{2}\right) = -i\sqrt{1 - \frac{\omega^2(\varepsilon_1 - \varepsilon_0)}{(ck_x)^2}}. \tag{15}$$

Figure 2(a) shows the TE and TM *confined guided modes* for the structure from Fig. 1(a), which correspond to real-k_x solutions of Eqs. (12)–(15). Graphically, real-k_x solutions are found by intersecting the blue (TE) and red (TM) curves [the left-hand sides of Eqs. (12)–(13) and Eqs. (14)–(15), respectively] with the black curve [the right-hand side of Eqs. (12)–(15)]. Since the TE and TM equations only differ in the factor $\frac{\varepsilon_0}{\varepsilon_1}$, which determines the slope of the tangent and cotangent functions but not the location of the branch cuts, the number of TE and TM confined modes is the same for any given index contrast, but TM modes are shifted to larger k_x values.

Panels (b) and (c) in Fig. 2 show, in addition to the confined modes, the TE and TM *leaky guided modes*, which correspond to complex-k_x solutions of Eqs. (12)–(15). It is evident from the figure that the TM resonances are closer to the real axis in comparison to the TE resonances, which implies that a larger fraction of the TM-modal intensity is confined to the core of the

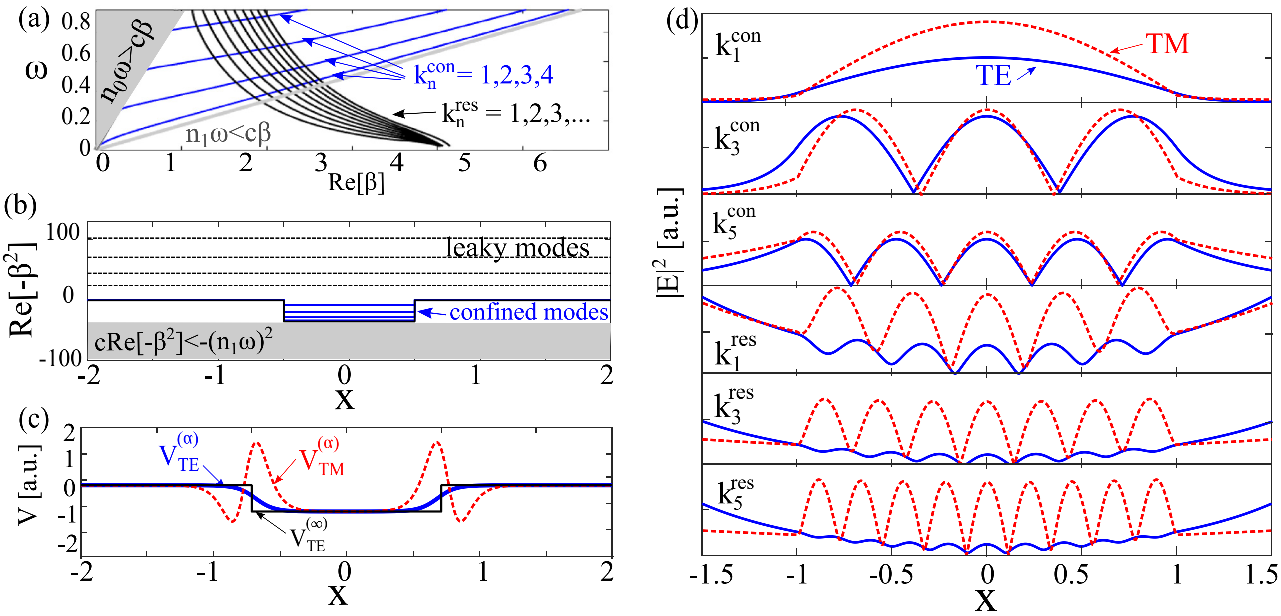

FIG. 3. (a) Dispersion relation (ω vs Re[β_n]) of TE modes, obtained by computing confined (blue) and leaky (black) propagation constants, β_n, at a range of frequencies, $0.01 < \frac{\omega L}{2\pi c} < 1$, for the structure from Fig. 1. Confined modes propagate in the core and decay in the cladding and satisfy $\omega\varepsilon_0 < \beta_n c < \omega\varepsilon_1$. The gray shaded area marks the light line of the cladding ($\beta_n c > \omega n_0$). (b) Confined (blue solid) and leaky (black dashed) TE modes and the TE potential (black solid) [Eq. (6) with $n(x)$ given by Eq. (17)], with $\frac{\omega L}{2\pi c} = 2$. (c) Smoothed TE (blue solid) and TM (red dotted) potentials, obtained by evaluating Eq. (6) and Eq. (16), respectively, using the smoothed index profile Eq. (18)]. (d) TE and TM confined and leaky mode profiles (blue solid and red dotted lines, respectively).

waveguide. Formally, the resonant wave vectors are the zeros of the functions $\mathcal{F}_{\rm TE}^{(e/o)}$ and $\mathcal{F}_{\rm TM}^{(e/o)}$, which are defined as the difference between the left- and right-hand sides of Eqs. (12)–(15). The superscript (e/o) denotes even or odd symmetry and the subscript denotes TE or TM polarization. Figure 2 shows the poles of $\Delta_{\rm TE} \equiv |\mathcal{F}_{\rm TE}^{(e)}|^{-2} + |\mathcal{F}_{\rm TE}^{(o)}|^{-2}$ and $\Delta_{\rm TM} \equiv |\mathcal{F}_{\rm TM}^{(e)}|^{-2} + |\mathcal{F}_{\rm TM}^{(o)}|^{-2}$. These poles are precisely the well-known scattering matrix poles, which can be derived directly from Maxwell's equations using electromagnetic scattering theory [26]. The location of the poles in the complex plane determines many physical properties, such as the scattering, absorption, and extinction cross sections. Note that despite the fact that we expect, based on Fig. 2(a), to find three real-k_x solutions both in the TE and TM polarizations, panels (b) and (c) show spurious real-k_x solutions [e.g., the pole on the real axis in (b) at $k_x \approx 2$]. These additional poles are an artifact of our numerical procedure, since we plot contours of the inverse squared modulus of the boundary-condition equations and not the equations themselves.

We conclude this section by discussing the dispersion relation of the guided modes, presented in Fig. 3(a). Confined guided modes propagate inside the core and decay in the cladding. Since these modes have real k_x and imaginary q, the (real) propagation constant, β_n, must be above the light line of the core ($\beta_n c < \omega n_1$) and below the light line of the cladding ($\beta_n c > \omega n_0$) [12] [see Eq. (10) and Eq. (11)]. In contrast, leaky guided modes decay also inside the core, i.e., they have complex q and k_x. The propagation constants of the lowest-order leaky modes still sit above the light line of the core, but at higher orders or smaller frequencies, we find modes below the light line, as demonstrated in Fig. 3(a) when the red curves penetrate the line Re[β_n]$c = \omega n_1$.

IV. SCALAR MAXWELL EQUATIONS AS SCHRÖDINGER-TYPE EQUATIONS

Apart from a very limited number of analytically solvable geometries, such as the piecewise continuous geometry of our example system, it is generally impossible to construct simple transcendental equations and one must solve Eq. (4) and Eq. (8) directly. Since the TE Maxwell equation is a Schrödinger-type equation, it can be solved using standard approaches from quantum mechanics. Although the TM equation contains a nonconservative force term [see discussion following Eq. (8)], we can recast it as a Schrödinger-type equation by introducing the transformation: $h_y(x) = n(x)\psi(x)$. We find that the new field ψ satisfies Eq. (5) with the effective potential

$$V_{\rm TM}(x) = -\left(\frac{\omega}{c}\right)^2 n^2(x) - \frac{1}{n}\frac{d^2n}{dx^2} + 2\left(\frac{1}{n}\frac{dn}{dx}\right)^2. \qquad (16)$$

More generally, one can apply similar tricks to transform the full-vector Maxwell equation into a Schrödinger-type equation, even in the absence of mirror-plane symmetry (for details, see lecture 3 in [31]).

The analogy to quantum mechanics offers a simple interpretation for the nature of the TE and TM solutions. The index profile of the rectangular waveguide [Fig. 1(a)] can be written as

$$n(x) = n_0 + (n_1 - n_0)\left[H\left(\frac{L}{2} + x\right) + H\left(\frac{L}{2} - x\right) - 1\right], \qquad (17)$$

where $H(x)$ is the Heaviside step function. The TE potential [Eq. (6)] with $n(x)$ given by Eq. (17) is equivalent to a one-dimensional square well. Confined modes are analogous to bound states in quantum mechanics, and their real propagation constants are in the range $-\omega^2 n_1^2 < -\beta_n^2 < -\omega^2 n_0^2$ (i.e., between the bottom of the well and the "ionization threshold"), as shown in Fig. 3(b). The effective TM potential [Eq. (16)] with $n(x)$ given by Eq. (17) is equivalent to a square-well potential with barriers of infinite height at the well boundaries. In order to visualize these barriers, we introduce the smoothed index profile:

$$n_\alpha(x) = n_0 + \frac{n_1 - n_0}{2}\left\{\tanh\left[\alpha\left(x + \frac{L}{2}\right)\right] + \tanh\left[\alpha\left(x - \frac{L}{2}\right)\right]\right\}, \tag{18}$$

which converges to $n(x)$ in the limit of $\alpha \to \infty$. The TE and TM effective potentials, $V_{\rm TE}^{(\alpha)}$ and $V_{\rm TM}^{(\alpha)}$, respectively, with smoothing parameter $\alpha = 25$ are shown in Fig. 3(c). The barriers in the TM potential give rise to constructive interference of the scattered light and produce a higher intensity inside the waveguide in comparison to TE modes. This point is demonstrated in Fig. 3(d), which shows three even confined modes and the first three leaky modes in the TE (blue solid lines) and TM (red dashed lines) polarizations.

V. RESONANCE STRUCTURE IN THE TE AND TM DENSITY OF STATES

In non-Hermitian quantum mechanics, resonances are associated with peaks in the density of energy states [usually denoted as $\rho_{(E)}$]. In nondegenerate systems with weak loss or gain, the density of states is given by a sum over δ-function peaks at bound-state energies and Lorentzian peaks at resonant energies. In non-Hermitian waveguides, the density of states is similarly defined as

$$\rho(\beta) = \sum_n \delta\left(\beta^2 - \left[\beta_n^2\right]^{\rm con}\right) + \sum_n {\rm Im}\frac{1}{\left[\beta_n^2\right]^{\rm res} - \beta^2}. \tag{19}$$

The first sum contains confined modes and the second contains the leaky modes. The latter sum becomes a set of Lorentzian peaks in the limit of isolated resonances (i.e., when ${\rm Re}[\beta_n^2] \gg {\rm Im}[\beta_n^2]$), since in this limit

$${\rm Im}\frac{1}{\beta_n^2 - \beta^2} \approx -\frac{{\rm Im}([\beta_n])/2\,{\rm Re}[\beta_n]}{(\beta - {\rm Re}[\beta_n])^2 + ({\rm Im}[\beta_n])^2}. \tag{20}$$

The density of states of TE and TM leaky modes is plotted in Fig. 1(c) for the structure from panel (a). The modal structure is evident in the TM case and is absent in the TE spectrum.

When the waveguide is excited at a specific location (x_0, z_0) (instead of homogeneously over the entire transverse cross section), the system's response is determined by the local density of states, which is defined as [32]

$$\rho_{\rm local}(x,\beta) = -{\rm Im}\left[\sum_n \frac{1}{\beta^2 - \beta_n^2}\frac{\psi_n^R(x)\psi_n^L(x)}{\int dx\,\psi_n^L(x)\psi_n^R(x)}\right]. \tag{21}$$

Equation (21) includes both leaky and confined modes in the summation and denotes the right and left eigenvectors of Maxwell operators [Eq. (4) and Eq. (8)] by ψ_n^R and ψ_n^L, respectively [25]. Since Maxwell's equations have the form of a symmetric generalized eigenvalue problem [33], the left and right eigenvectors are equal. In order to evaluate the denominator of Eq. (21), some care needs to be taken to handle the divergence of the leaky modes at $x = \pm\infty$. It turns out that the modes are properly normalized by omitting the outer limits of integration:

$$\int_{-\infty}^{\infty} \varepsilon(x)\psi_n^2(x)dx = \int^{-L/2} \varepsilon_0\psi_n^2(x)dx + \int_{-L/2}^{L/2} \varepsilon(x)\psi_n^2(x)dx + \int_{L/2} \varepsilon_0\psi_n(x)dx. \tag{22}$$

(A rigorous proof of this normalization approach can be found in [25] and [17].) Substituting Eq. (9) into Eq. (22), we obtain in our case

$$\int_{-\infty}^{\infty} dx\,\psi(x)^2 = \frac{e^{-iqL}}{iq} + \left(A^2\frac{k_xL + \sin k_xL}{2k_x} + B^2\frac{k_xL - \sin k_xL}{2k_x}\right). \tag{23}$$

Figure 4 shows the normalized local density of states $\rho_{\rm local}(x,\beta)$ [Eq. (21)] for TE and TM modes [panels (a) and (b), respectively] of the structure from Fig. 1. The local density of states vanishes at nodes of the field (black regions) and peaks at field maxima (yellow regions). In the TM case, strong peaks are seen near resonant wave vectors.

VI. DISCUSSION

In this paper, we explored the polarization dependence of the propagation distance in *perfectly straight real-index*

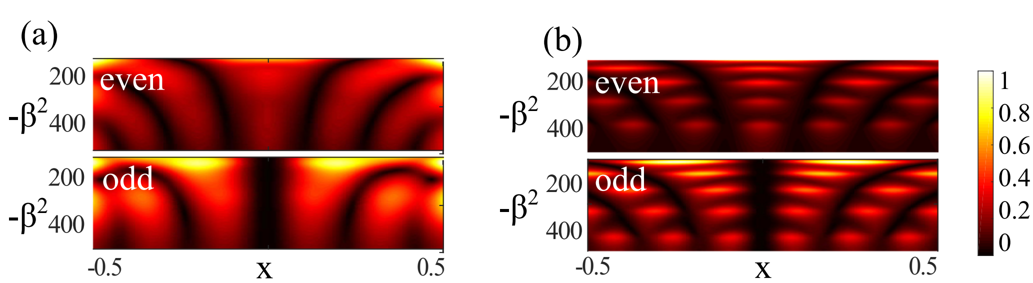

FIG. 4. Normalized local density of states [Eq. (21)] for TE and TM modes [panels (a) and (b), respectively], for the structure from Fig. 1. The local density of states vanishes (black regions) at nodes of the modes and peaks at field maxima (yellow regions). In the TM case, strong peaks are seen near resonant wave vectors. The color scale is shown on the right.

waveguides. We focused on a special kind of modes, in which the imaginary part of the propagation constant is solely due to leakage of radiation in the transverse direction. Complex propagation constants are typically encountered in systems with a complex index of refraction, such as $\mathcal{PT}$-symmetric waveguides [5] with commensurate amounts of loss and gain, and in semiconductor lasers with nonlinear gain [34]. They also arise in waveguides with surface roughness or waveguides with small variation of the cross section along the waveguide axis [24]. In bent planar waveguides, the bend losses can be described by assigning an imaginary part to the propagation constant [35]. In this context, recent work by Bauters *et al.* showed that the TM modes in rectangular waveguides with a high aspect ratio are associated with ultralow bend losses [27,28]. This property of TM modes in bent waveguides is similar to our findings in straight waveguides.

Since straight real-index waveguides are much easier to fabricate than the other mentioned examples, they can be used to design simple experiments to test the predictions and applications of non-Hermitian optics. For example, one can use leaky-mode propagation to design simple and compact filters for TM-polarized light. While traditional TE or TM mode filters typically use composite structures, such as metal-clad and buffer layers [36], or anisotropic substrates [37], we propose using straight single-constituent waveguides. Consider a waveguide whose width L_x varies adiabatically as a function of z, so it consists of a wide and a narrow section. Let us choose the width of the wide section to have N confined modes, and the width of the narrow section to support only N-1 confined modes. When unpolarized light enters the thin section of the waveguide, the N'th confined modes become leaky modes, and TE components of the field decay much more rapidly than TM components. Therefore, after a short propagation in the thin section, the light becomes predominantly TM polarized. This simple design can be easily integrated on a microscale chip, since the thin section can be made very short assuming that the contrast between the TE and TM propagation constants is significant. Moreover, similar principles can be applied to design a multimode filter.

Another intriguing application of TM leaky resonances is communication between distant waveguides. Confined modes can only carry information between nearby waveguides. The separation between the waveguides cannot exceed the length of the evanescent tails because the coupling strength depends on the overlap between modes of the individual waveguides [38]. (See, for instance, Ref. [39], which shows Rabi oscillations between evanescently coupled waveguides.) By observing the leaky mode profiles in Fig. 3(d), we expect that leaky modes could convey information over many wavelengths of the light. TE resonances are not suitable for this task because the modes are delocalized and only a small fraction of the light actually propagates in the core of the waveguide. However, TM resonances are promising candidates for this task.

ACKNOWLEDGMENTS

A.P. is partially supported by an Aly Kaufman Fellowship at the Technion. N.M. acknowledges the financial support of I-Core: The Israeli Excellence Center "Circle of Light" and of the Israel Science Foundation Grant No. 1530/15. Finally, we would like to thank Sir M. V. Berry, S. G. Johnson, and E. Narevicius for insightful discussions.

[1] C. M. Bender and S. Boettcher, Real Spectra in Non-Hermitian Hamiltonians Having $\mathcal{PT}$ Symmetry, Phys. Rev. Lett. **80**, 5243 (1998).

[2] C. E. Ruter, K. G. Makris, R. El-Ganainy, D. N. Christodoulides, M. Segev, and D. Kip, Observation of parity–time symmetry in optics, Nat. Phys. **6**, 192 (2010).

[3] S. Klaiman, U. Gunther, and N. Moiseyev, Visualization of Branch Points in $\mathcal{PT}$-Symmetric Waveguides, Phys. Rev. Lett. **101**, 080402 (2008).

[4] K. G. Makris, R. El-Ganainy, D. N. Christodoulides, and Z. H. Musslimani, Beam Dynamics in $\mathcal{PT}$-Symmetric Optical Lattices, Phys. Rev. Lett. **100**, 103904 (2008).

[5] A. Guo, G. J. Salamo, D. Duchesne, R. Morandotti, M. Volatier-Ravat, V. Aimez, G. A. Siviloglou, and D. N. Christodoulides, Observation of $\mathcal{PT}$-Symmetry Breaking in Complex Optical Potentials, Phys. Rev. Lett. **103**, 093902 (2009).

[6] M. Brandstetter, M. Liertzer, C. Deutsch, P. Klang, J. Schöberl, H. E. Tureci, G. Strasser, K. Unterrainer, and S. Rotter, Reversing the pump dependence of a laser at an exceptional point, Nat. Commun. **5**, 4034 (2014).

[7] Z. Lin, H. Ramezani, T. Eichelkraut, T. Kottos, H. Cao, and D. N. Christodoulides, Unidirectional Invisibility Induced by $\mathcal{PT}$-Symmetric Periodic Structures, Phys. Rev. Lett. **106**, 213901 (2011).

[8] I. Vorobeichik, M. Orenstein, and N. Moiseyev, Intermediate-mode-assisted optical directional couplers via embedded periodic structure, IEEE J. Quantum Electron. **34**, 1772 (1998).

[9] J. Doppler, A. A. Mailybaev, J. Bohm, U. Kuhl, A. Girschik, F. Libisch, T. J. Milburn, P. Rabl, N. Moiseyev, and S. Rotter, Dynamically encircling an exceptional point for asymmetric mode switching, Nature (London) **537**, 76 (2016).

[10] J. J. Wiersig, Enhancing the Sensitivity of Frequency and Energy Splitting Detection by Using Exceptional Points: Application to Microcavity Sensors for Single-Particle Detection, Phys. Rev. Lett. **112**, 203901 (2014).

[11] A. W. Snyder and J. Love, *Optical Waveguide Theory* (Springer Science and Business Media, New York, 2012).

[12] J. D. Joannopoulos, S. G. Johnson, J. N. Winn, and R. D. Meade, *Photonic Crystals, Molding the Flow of Light* (Princeton University Press, Princeton, NJ, 2008).

[13] M. Skorobogatiy and J. Yang, *Fundamentals of Photonic Crystal Guiding* (Cambridge University Press, Cambridge, UK, 2009).

[14] J. Hu and C. R. Menyuk, Understanding leaky modes: Slab waveguide revisited, Adv. Opt. Photon. **1**, 58 (2009).

[15] P. T. Leung, S. Y. Liu, and K. Young, Completeness and orthogonality of quasinormal modes in leaky optical cavities, Phys. Rev. A **49**, 3057 (1994).

[16] K. M. Lee, P. T. Leung, and K. M. Pang, Dyadic formulation of morphology-dependent resonances. I. Completeness relation, JOSA B **16**, 1409 (1999).

[17] A. Pick, B. Zhen, O. D. Miller, C. W. Hsu, F. Hernandez, A. W. Rodriguez, M. Soljacic, and S. G. Johnson, General theory of spontaneous emission near exceptional points, Opt. Exp. **25**, 12325 (2017).

[18] S. Y. Lee, J. W. Ryu, J. B. Shim, S. B. Lee, S. W. Kim, and K. An, Divergent Petermann factor of interacting resonances in a stadium-shaped microcavity, Phys. Rev. A **78**, 015805 (2008).

[19] P. T. Kristensen, C. van Vlack, and S. Hughes, Generalized effective mode volume for leaky optical cavities, Opt. Lett. **37**, 1649 (2012).

[20] N. Marcuvitz, *Waveguide Handbook* (Peter Peregrinus Ltd., London, 1951), p. 39.

[21] L. Novotny and C. Hafner, Light propagation in a cylindrical waveguide with a complex, metallic, dielectric function, Phys. Rev. E **50**, 4094 (1994).

[22] K. H. Chlereth and M. Tacke, The complex propagation constant of multilayer waveguides: An algorithm for a personal computer, IEEE J. Quantum Electron. **26**, 627 (1990).

[23] E. Anemogiannis and E. N. Glytsis, Multilayer waveguides: Efficient numerical analysis of general structures, J. Light. Technol. **10**, 1344 (1992).

[24] I. Vorobeichik, U. Peskin, and N. Moiseyev, Modal losses and design of modal irradiance patterns in an optical fiber by the complex scaled (t,t') method, JOSA B **12**, 1133 (1995).

[25] N. Moiseyev, *Non-Hermitian Quantum Mechanics* (Cambridge University Press, Cambridge, UK, 2011).

[26] R. G. Newton, *Scattering Theory of Waves and Particles* (Springer Science & Business Media, New York, 2013).

[27] J. F. Bauters, M. J. R. Heck, D. John, D. Dai, M. C. Tien, J. S. Barton, A. Leinse, R. G. Heideman, D. J. Blumenthal, and J. E. Bowers, Ultra-low-loss high-aspect-ratio Si_3N_4 waveguides, Opt. Express **19**, 3163 (2011).

[28] D. Dai, Z. Wang, J. F. Bauters, M. C. Tien, M. J. R. Heck, D. J. Blumenthal, and J. E. Bowers, Polarization characteristics of low-loss nano-core buried optical waveguides and directional couplers, in *Group IV Photonics (GFP), 2010 7th IEEE International Conference* (IEEE, New York, 2010), pp. 260–262.

[29] We use the identity $\varepsilon \frac{d}{dx}\frac{1}{\varepsilon}\frac{d}{dx}h_y = -\frac{\varepsilon'}{\varepsilon}\frac{dh_y}{dx} + \frac{d^2h_y}{dx^2} = -\frac{d\ln n^2}{dx}\frac{dh_y}{dx} + \frac{d^2h_y}{dx^2}$.

[30] S. Gasiorowicz, *Quantum Physics* (John Wiley & Sons, New York, 2007).

[31] M. V. Berry, Classical adiabatic angles and quantal adiabatic phase, J. Phys. A: Math. Gen. **18**, 15 (1985).

[32] A. Taflove, A. Oskooi, and S. G. Johnson, Advances in FDTD computational electrodynamics: Photonics and nanotechnology, p. 76, available online at http://arxiv.org/ftp/arxiv/papers/1301/1301.5366.pdf.

[33] The symmetry of Maxwell's operator can be seen from its equivalence to a symmetric Schrodinger-type equation.

[34] A. P. Bogatov, A. E. Drakin, V. R. Medvedev, and A. V. Ustinov, Calculation of the propagation constant of a laser mode in multilayer quantum-well heterostructure by the 'incoming' wave method, Quant. Electron. **28**, 474 (1998).

[35] J. Lu, S. He, and V. G. Romanov, A simple and effective method for calculating the bending loss and phase enhancement of a bent planar waveguide, Fiber Integrat. Opt. **24**, 25 (2005).

[36] S. Ohke, T. Umeda, and Y. Cho, TM-mode selective filter using leaky waveguide structure, Electron. Commun. Jpn. 2 **85**, 9 (2002).

[37] T. P. Sosnowski, Polarization mode filters for integrated optics, Opt. Commun. **4**, 408 (1972).

[38] H. A. Haus and W. Huang, Coupled-mode theory, Proc. IEEE **79**, 1505 (1991).

[39] M. Ornigotti, G. Della Valle, T. T. Fernandez, A. Coppa, V. Foglietti, P. Laporta, and S. Longhi, Visualization of two-photon Rabi oscillations in evanescently coupled optical waveguides, J. Phys. B **41**, 085402 (2008).